Molecular-dynamics simulations of slow copper cluster deposition

Lee Rongwu and Pan Zhengying
Physics Department 2, Fudan University, Shanghai 200433, China
and Ion Beam Laboratory, Shanghai Institute of Metallurgy, Academic Sinica, China

Ho Yukun
China Center of Advanced Science and Technology (World Laboratory), P.O. Box 8730, Beijing, China
and Physics Department 2, Fudan University, Shanghai 200433, China
(Received 20 June 1995; revised manuscript received 5 September 1995)

In this paper, the dynamic process of $(Cu)_{13}$ cluster deposition on copper substrate is investigated by molecular-dynamics simulations, in which a many-body hybrid potential by combining the Molière potential with the tight-binding potential is used to describe the interactions among copper atoms. The initial energy of the cluster ranges from 2 to 20 eV per atom. By taking ''snapshots'' and analyzing the energy partition during the deposition process, we find that the cluster atoms could rearrange from the original icosahedral structure to the fcc structure and form epitaxial layers at the end of the simulations. The penetration depths of the cluster atoms increase with the impact energy. The substrate suffers radiation damage when the impact energy of the cluster increases over a value around 20 eV/atom. The energy analyses show that the cluster atoms activate the substrate atoms in the impact region through collective collisions in a very short time (some tenth picoseconds) by providing energies for the migration and reconstruction.

I. INTRODUCTION

Recently, the cluster-substrate interaction has attracted much attention as a promising method for growing high-quality films at low substrate temperatures.[1–3] In contrast to the conventional ion-beam deposition, the ionized-cluster beam has higher effective beam density because of its higher ratio of mass to charge. The ionized-cluster beam deposition (ICBD) could provide sufficient localization energy to stimulate the surface atoms to form high-quality films with less surface damage. Yamamura[4] studied the collision phase of ICBD using the binary collision approximation simulations and the molecular-dynamics (MD) simulations with the pairwise potential. Kwon *et al.*[5] studied the growth of Si on Si(111) by means of MD simulations with a many-body potential. However, many aspects of the ICBD mechanism are still not well understood. In this paper, we investigate the dynamic process of copper cluster deposition on copper substrate using MD simulations. Particular attention is paid to the microscopic characteristics of the deposition process, the energy effect on the quality of growing films and the rearrangement of the cluster atoms. In order to understand the whole ICBD process, which includes both the collision and the relaxation phases, a hybrid potential[6] combining Molière potential[7] with tight-binding (TB) potential[8] is used to describe the interactions among copper atoms. Section II briefly describes the MD simulation model used in our study. The results and discussion are presented in Sec. III.

II. SIMULATION MODEL

A. Interaction potential and geometric structure of $(Cu)_{13}$ cluster

In this study, the atomic energy concerned ranges from under a tenth of an eV to more than tens of eV per atom. It is known that TB potential is able to reproduce the structure, the bulk and the surface properties of transition and noble metals, and the calculated variances of atomic mean-square displacements within the normal temperature scope are also consistent with the experimental results.[8,9] Thus TB potential is suitable at the lower-energy regime, while the pairwise potential, such as the Molière potential, is applicable at the higher-energy regime. To span the entire energy regime of relevant interactions, a hybrid potential[6] is adopted to describe the interactions among copper atoms. The potential energy of an atom i in the hybrid potential contains two components written as E_b^i and E_r^i, respectively, where E_b^i is an attractive energy, which is the same as that in TB potential, i.e.,

$$E_b^i = -\left[\sum_{j\neq i} \xi^2 e^{-2q(r_{ij}/d_0-1)}\right]^{1/2}. \tag{1}$$

TABLE I. Potential parameters.

ξ (eV)	q	d_0 (Å)	A (eV)	p	r_1 (Å)	r_2 (Å)	B_m (eV)	a_f (Å)
1.2291	2.282	0.254 66	0.0869	10.83	2.1	1.4	0.000 121 1	0.0738

However, the repulsive pair potential E_r^i is a combination of the repulsive part in the TB potential with the Molière potential, smoothly connecting these two components at the intermediate distance with a cubic spline, given as follows:

$$E_r^i = \sum_{j \neq i} V_r(r_{ij}) \tag{2}$$

and

$$V_r(r) = \begin{cases} Ae^{-p(r/d_0-1)}, & r \geqslant r_1 \\ A_0 + A_1 r + A_2 r^2 + A_3 r^3, & r_1 > r > r_2 \\ B_m(0.35e^{-0.3r/a_f} + 0.55e^{-1.2r/a_f} + 0.10e^{-6.0r/a_f})/r, & r \leqslant r_2, \end{cases} \tag{3}$$

where r_{ij} is the interdistance between the atom i and atom j and d_0 is the nearest-neighbor distance. The parameters ξ, q, d_0, A, and p are adjusted to fit the cohesive energy and the elastic constants of the bulk copper, A_0, A_1, A_2, and A_3 are the fit coefficients. The choice of the fitting distances r_1 and r_2 is made carefully to get a reasonable curvature in the region between r_1 and r_2. The parameters in the hybrid potential are given in Table I. To examine the hybrid potential, we calculate the lattice constant and the cohesive energy of copper metal and find that the results are consistent with the experimental data.

The structure and the cohesive energy of a $(Cu)_{13}$ cluster must be considered since what we are concerned with is the cluster impact at relatively low energies (2–20 eV/atom). To do that, we must first verify whether the hybrid potential used is suitable for describing the cluster atomic interactions. First, we calculate the bond length and the bond energy of the diatomic copper molecule and get 2.22 Å and 1.30 eV, respectively, while the experimental data are 2.22 Å (Ref. 10) and 1.02 eV,[11] respectively, which shows that this potential gives the bond length correctly but overestimates the bond energy slightly. Second, through optimizing the total cluster energy in its nuclear configuration space, we get the icosahedral and the double icosahedral structures of the stable 13- and 19-atom clusters using this potential. These structures are consistent with both the experimental and the theoretical results for transition-metal clusters.[12,13] The above shows that this hybrid potential can be used to describe the copper clusters. Some previous researches usually employed[6,14] an approximately spherical fcc structure including a center atom and its nearest neighbors for $(Cu)_{13}$, where the mean number of the nearest atoms is 5.5 and the mean cohesive energy is 2.48 eV/atom, whereas in our calculated icosahedral structure of a $(Cu)_{13}$ cluster, the mean number of the nearest atoms is 6.5 and the mean cohesive energy is 2.60 eV/atom. As generally believed, a greater average number of neighbor atoms and a higher cohesive energy correspond to a more stable structure. Thus it is appropriate for us to adopt the icosahedral structure for $(Cu)_{13}$. In Figs. 1(a) and 1(b), the fcc and the icosahedral structures of $(Cu)_{13}$ are presented, respectively.

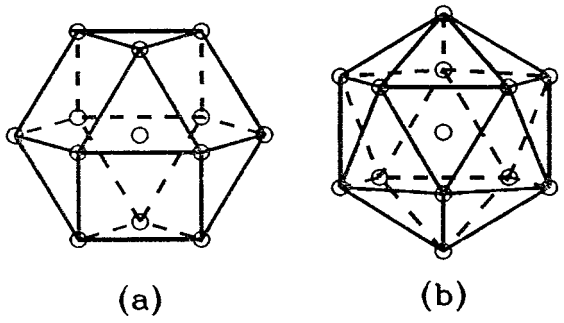

FIG. 1. The structure of $(Cu)_{13}$. (a) fcc structure, (b) icosahedral structure.

B. Computational model

The computational model used is similar to that in Ref. 15. The copper substrate has fcc structure with dimensions of $10a_0 \times 10a_0 \times 6a_0$ (a_0 is the lattice constant). The origin of the coordinate system is put at the center of the substrate. At the beginning of each event, the icosahedron $(Cu)_{13}$ cluster is initially located at a sufficient distance above the substrate surface to have negligible interaction with the substrate surface, and aims at the center of the substrate to avoid any possible rotation of the simulated system in the direction with a polar angle $\theta = 10°$ and an azimuthal angle $\phi = 8°$ impacting on Cu(001) surface. We simulate the events with impact energies of $E_0 = 2$, 5, 10, 15, and 20 eV per atom, respectively. Each simulated event lasts 10 ps, which covers both the collision and the relaxation phases.

III. RESULTS AND DISCUSSION

We begin with studying the cluster-substrate interaction of a 5-eV/atom $(Cu)_{13}$ cluster with Cu substrate to explore the whole deposition process. Figure 2 exhibits the side views of the atomic locations in the x-z plane at several instants during the impact event. For clarity, only atoms within a slab containing four atomic layers around the substrate center are included in that figure, in which a cluster atom is shown as a small circle and a substrate atom as a dot. It is seen in Fig. 2(b) that the cluster frontier arrives at the substrate surface at about 0.05 ps. Then the cluster depresses the substrate through collective collisions and the original structures of both the cluster and the substrate surface are distorted [Fig. 2(c)]. At about 0.35 ps [Fig. 2(d)], the dissociation of the cluster and the local disruption of the substrate surface become pronounced. Subsequently, the cluster atoms rebound together with the substrate atoms in the impact region [Figs. 2(e) and 2(f)]. After about 1 ps, atoms in the collision zone oscillate and migrate towards their equilibrium states [Figs. 2(g) and 2(h)]. At about 4 ps [Fig. 2(i)], an epitaxial layer is

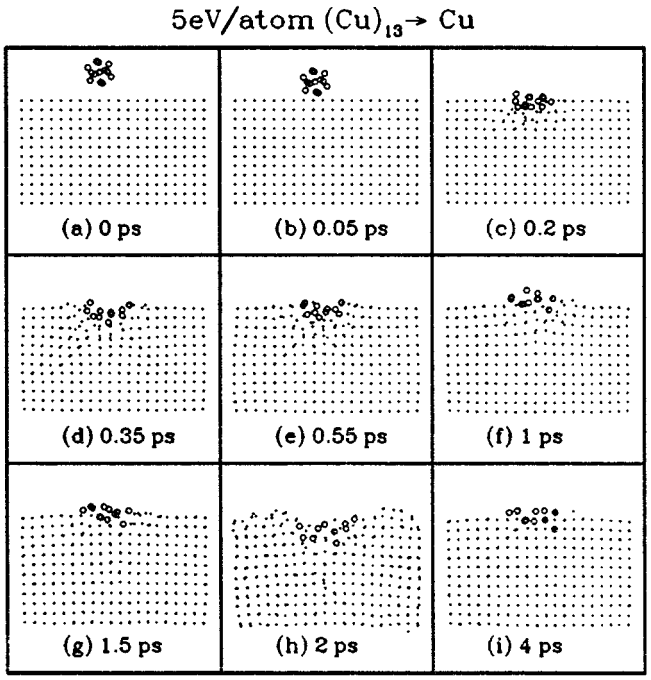

FIG. 2. Sequential snapshots of locations of the cluster atoms (small circles) and the substrate atoms (dots) in x-z plane for an event of a 5-eV/atom $(Cu)_{13}$ cluster impact on a Cu substrate.

formed, which has the same fcc structure as that of the original Cu substrate. At the end of the simulation, we find no point defect in either the substrate or the epilayer, no cluster atom migrating a significant distance over the substrate, and no substrate atom sputtered.

In order to investigate the evolution of the system surface structure during the deposition process, the pair correlation function $g(r)$ of the atoms within a small box of $4a_0\times 4a_0\times 2a_0$ in the surface around the collision center is calculated, and $g(r)$ is defined as

$$g(r)=6V(4\pi)^{-1}N^{-2}\left[\sum_{i=1}^{N}\sum_{j=i+1}^{N}\delta(r_{ij}-r)\right]\times[(r+\delta r)^3_{\delta r\to 0}-r^3]^{-1}, \tag{4}$$

where V is the crystal volume concerned, N denotes the atom number within V, and r_{ij} is the interdistance between atoms i and j. Obviously, $g(r)$ represents the probability density function versus atomic interdistance r. Thus, the areas under the peaks of the $g(r)$ curve give the coordination numbers, and hence the sharpness and the separation of the peaks present the ordering extent of atomic arrangement. Figures 3(a), 3(b), and 3(c) depict the pair-correlation functions of the atoms in the surface impact region at the time before the impact ($t=0$ ps), the time when the maximum depression of the substrate surface occurs ($t\approx 0.35$ ps) and the time after the full relaxation ($t\approx 4$ ps), respectively. At $t=0$ ps, the surface impact region has a standard fcc structure with no thermal vibration. In Fig. 3(b) ($t\approx 0.35$ ps), only the first peak is distinguishable. But in Fig. 3(c) ($t\approx 4$ ps) significant peaks appear again, although they are not as clear as those in Fig. 3(a) because of the impact-induced atomic thermal vibration. Figure 3 clearly shows the disruption and the reconstruction of the substrate surface during the deposition process.

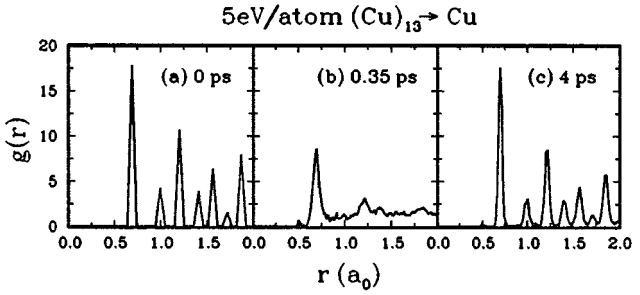

FIG. 3. The pair correlation function $g(r)$ for atoms of the impact region for an event of 5- eV/atom $(Cu)_{13}$ cluster impact on a Cu substrate. (a) $t=0$ ps (with standard fcc structure and no consideration of thermal vibration), (b) $t=0.35$ ps, and (c) $t=4$ ps.

Figures 4–6 present the various energies of the substrate and the cluster versus time. These are statistical results for 10 events with the same impact energy (5 eV/atom), which show the energy deposition and partition characteristics during the cluster impact process. The orientation and the impact position of the cluster with respect to the substrate surface are randomly chosen at the beginning of each event. The simulation of each event covers 1 ps, since the major energy change in each event occurs at the stage of the collision cascade, which generally lasts less than 1 ps.

Figure 4 shows the energy transfer process from the cluster to the substrate. In Fig. 4, $\Delta E_{\rm tt}$ and $\Delta E_{\rm ct}$ denote the total energy changes of the substrate and the cluster, respectively. We can see that the cluster transfers most of its energy to the substrate within the first 0.4 ps. After 0.4 ps, the very small values of $\Delta E_{\rm tt}$ and $\Delta E_{\rm ct}$ indicate that the cluster atoms and the substrate impact zone atoms are nearly in the state of thermal equilibrium. It is worth mentioning that the energy transfer takes place almost within the same period of time for all simulated events with various impact energies.

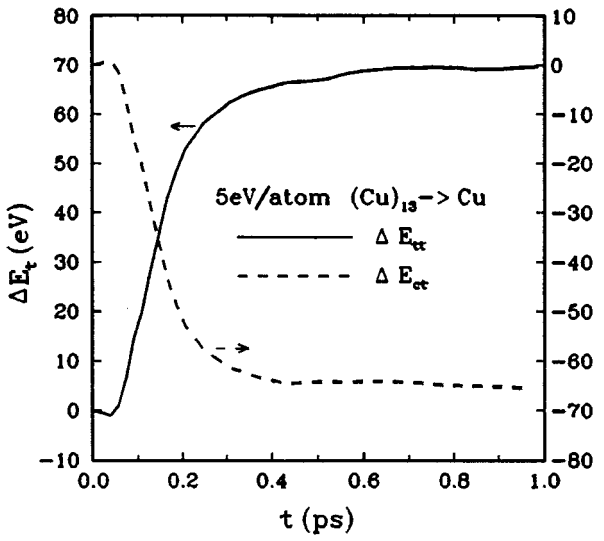

FIG. 4. The total energy changes of the substrate ($\Delta E_{\rm tt}$) and the cluster ($\Delta E_{\rm ct}$) vs time for an event of a 5-eV/atom $(Cu)_{13}$ cluster impact on a Cu substrate [$\Delta E_{\rm tt}\,(t=0)=\Delta E_{\rm ct}\,(t=0)=0$].

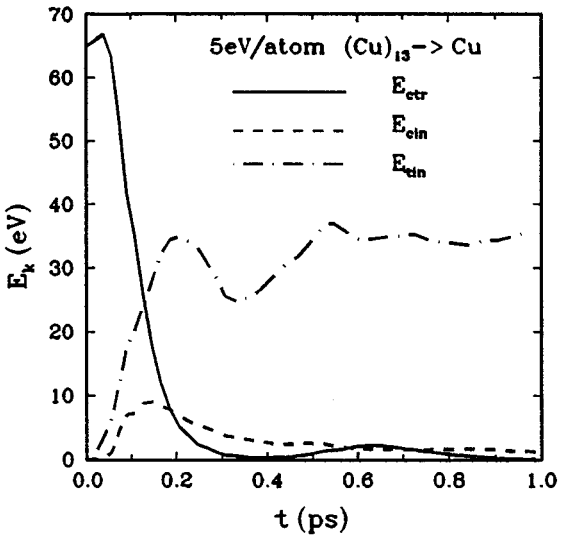

FIG. 5. The translational energy (E_{ctr}) and the internal energy (E_{cin}) of the Cu cluster and the internal energy of the substrate (E_{tin}) vs time for an event of a 5-eV/atom $(Cu)_{13}$ cluster impact on a Cu substrate.

Figure 5 exhibits the kinetic energies of both the cluster and the substrate versus time. It shows the energy partition during the impact process. In Fig. 5, E_{ctr} is the kinetic energy of the cluster center of mass, and E_{cin} and E_{tin} are the internal energies of the cluster and the substrate, respectively. It can be seen that most of the initial cluster translational energy converts into the internal energies of the cluster and the substrate atoms at the early stage of collision cascade ($t \approx 0.15$ ps), when all cluster atoms reach the surface and a local high-density collision cascade zone is formed. The cluster dissociation usually occurs at the same time. Then the internal energy of the atoms in the compressed zone is released. We can see that there are temporal oscillations of E_{tin}, which correspond to the reverse oscillations of the substrate potential-energy change ΔE_{tp} (see Fig. 6), and the amplitudes of the oscillations decline with time. Because of the energy conversion between the kinetic energy and the potential energy, the energy oscillations reflect the surface vibration caused by the bombardment of the cluster. With the system approaching the equilibrium state, the surface vibration becomes weaker.

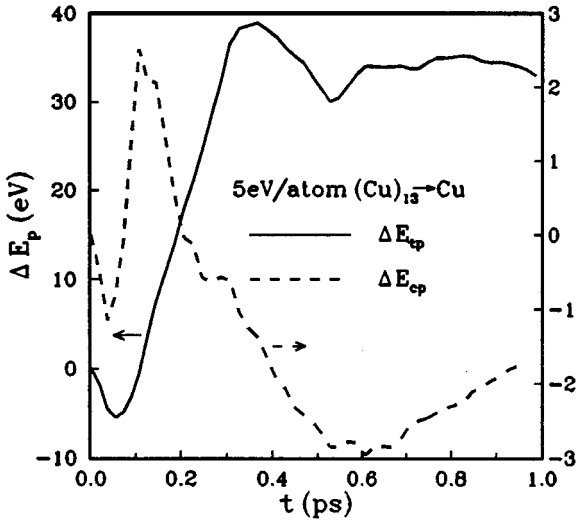

FIG. 6. The potential-energy changes of the substrate (ΔE_{tp}) and the cluster (ΔE_{cp}) vs time for an event of a 5-eV/atom $(Cu)_{13}$ cluster impact on a Cu substrate [$\Delta E_{tp}\,(t=0)=\Delta E_{cp}\,(t=0)=0$].

Figure 6 shows the configuration changes of both the cluster and the substrate. In Fig. 6, ΔE_{tp} and ΔE_{cp} denote the total potential energy changes of the substrate and the cluster, respectively. Initially, when the cluster reaches the substrate surface, both ΔE_{tp} and ΔE_{cp} decrease slightly because the interaction between the cluster and the substrate is mainly attractive. Then the cluster begins to depress the substrate, and ΔE_{tp} and ΔE_{cp} increase because the surface repulsive barrier plays a major role. At about 0.35 ps, when the maximum depression of the substrate surface occurs [also see Fig. 2(d)], ΔE_{tp} reaches its maximum value. Then the system enters the relaxation phase, where ΔE_{tp} oscillates, but the total energy is conserved.

It is interesting to examine the potential-energy change of the cluster atoms (ΔE_{cp}) in Fig. 6. First ΔE_{cp} increases when the cluster deformation occurs, then it decreases and oscillates around a value much lower than that when the cluster frontier just reaches the substrate surface. This means that after the dissociation of the cluster, the cluster atoms rearrange according to fcc structure, which has a higher cohesive energy (3.35 eV/atom) than that of the cluster original icosahedral structure (2.60 eV/atom). To further the investigation of the rearrangement phenomenon, we also explore the $(Cu)_{13}$ deposition at the impact energy of 0.5 eV/atom, which is much lower than the cluster mean cohesive energy 2.60 eV/atom. We find that the cluster seems to melt on the substrate surface, and form two typical epitaxial layers of fcc structure with no atom penetration at such impact energy. This means that the rearrangement of cluster atoms takes place automatically in the deposition process because of the difference between the mean cohesive energy of the cluster and that of the substrate. The existing experiments also support our results that the cluster atoms rearrange themselves on substrate surface to form a fcc structure.[16]

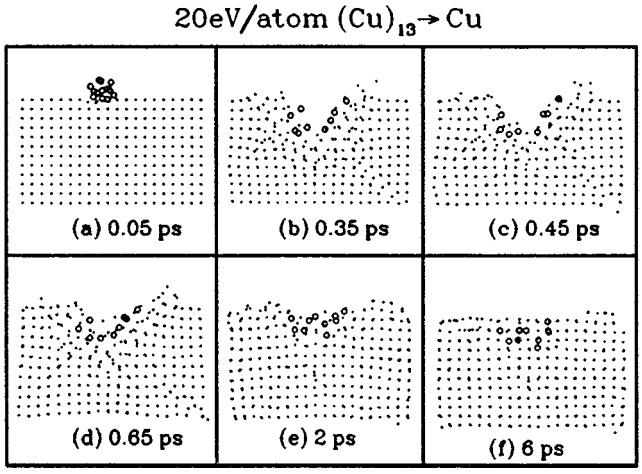

FIG. 7. The same as in Fig. 2, but for an impact energy of 20 eV/atom.

TABLE II. The depth distributions of the cluster atoms, vacancies, and interstitials at the end of several simulation events for a $(Cu)_{13}$ cluster impacting on a Cu substrate. In the table a, b, c, d, e, and f denote the impact events with energies of 0.5, 2, 5, 10, 15, and 20 eV per atom, respectively. S_i is the ith substrate layer below the surface ($i=1$ is the surface layer) and e_i is the ith epilayer above s_1.

	Cluster atoms						Vacancies						Interstitials					
	a	*b*	*c*	*d*	*e*	*f*	*a*	*b*	*c*	*d*	*e*	*f*	*a*	*b*	*c*	*d*	*e*	*f*
e_1	3	1																
e_2	10	10	8	4	4													
s_1		2	4	5	3	2						2						
s_2			1	4	4	6												
s_3					1	4												
s_4					1	1												2
s_5																		3

The 5-eV/atom cluster deposition discussed above is a typical example where high-quality films could be grown. With the increase of incident energy, the disordered collision region (crater and so on) becomes even wider and deeper. Figure 7 presents the side views of the atomic locations for $E_0=20$ eV/atom. A pronounced transient crater with a diameter up to $\sim 8a_0$, which is much larger than the size of a $(Cu)_{13}$ cluster, is produced due to the higher impact energy. It is worthwhile to note that the cluster atoms are almost fully embedded into the substrate surface, replacing the substrate atom positions in the layers beneath the surface, and some original substrate atoms are forced onto the surface to form the epitaxial layers after relaxation. Although the impact region reconstructs at the end of the simulation, the damage cannot be completely eliminated: a few substrate atoms become interstitial atoms and some vacancies appear on the surface layer. This means that the cluster-substrate collision begins to create radiation damage when the cluster energy goes over a value around 20 eV/atom.

The effect of the cluster impact energy on the deposition can be seen in Table II, which gives the depth distributions of the cluster atoms, vacancies, and interstitials at the end of several simulation events for a $(Cu)_{13}$ cluster impacting on a Cu substrate. In this table, a, b, c, d, e, and f denote the impact events with energies of 0.5, 2, 5, 10, 15, and 20 eV per atom, respectively. s_i is the ith substrate layer below the surface ($i=1$ is the surface layer) and e_i is the ith epilayer above s_1. This table clearly illustrates the threshold effect of deposition, which is that high-quality films are formed at lower impact energies while radiation damage appears at higher impact energies.

IV. CONCLUSION

Our main results can be summarized as the following.

(1) The features of the cluster-solid interaction are far different from those of the single-particle-solid interaction. In the former case the collective collisions play a dominant role. The cluster depresses the substrate surface through the collective interactions and rapidly transfers most of its translational energy to the substrate within a few tenth picoseconds. In the meantime the cluster dissociates and disrupts the substrate impact zone where a transient crater appears, and the atoms in the impact zone are stimulated and get the migration energies that are important for their reconstruction and helpful for growing high-quality epitaxial layers.

(2) The deposition of $(Cu)_{13}$ on a Cu(001) surface could form high-quality epitaxial layers without any point defect left after relaxation at low impact energy (about 5 eV/atom). The penetration depths of the cluster atoms increase with the impact energy. The substrate suffers radiation damage when the impact energy of the cluster increases over a value around 20 eV/atom. This is the threshold phenomenon of the cluster deposition.

(3) We have observed the reconstruction of the cluster atoms during the deposition process. The reconstruction is very important for growing high-quality thin film, especially for the film growth with multicomponents and more complicated structure, which we plan to study in the future. It also shows that the potential and the physical model used here are correct.

ACKNOWLEDGMENTS

This work was supported by the National Natural Science Foundation of China and the Joint Laboratory for Material Modification by Laser, Ion and Electron Beams, Dalian University of Technology.

[1] I. Yamada, H. Taksoka, H. Usui, and T. Takagi, J. Vac. Sci. Technol. A **4**, 722 (1986).

[2] R. Beuhler and L. Friedman, Chem. Rev. **86**, 521 (1986).

[3] H. Hsieh, R. S. Averback, H. Sellers, and C. P. Flynn, Phys. Rev. B **45**, 4417 (1992).

[4] Y. Yamamura, Nucl. Instrum. Methods. B **45**, 707 (1990).

[5] I. Kwon, R. Biswas, G. S. Grest, and C. M. Soukoulis, Phys. Rev. B **41**, 3678 (1990).

[6] M. Hou and Z. Pan, Nucl. Instrum. Methods Phys. Res. Sect. B (to be published).

[7] M. T. Robinson and I. M. Torrens, Phys. Rev. B **9**, 5008 (1974).

[8] B. Loisel, D. Gorse, and V. Pontikis, Surf. Sci. **221**, 365 (1989).

[9] V. Rosato, M. Guillope, and B. Legrand, Philos. Mag. A **59**, 321 (1989).
[10] N. W. Ashcroft and N. D. Mermin, *Solid State Physics* (Holt, Reinehart and Winston, New York, 1976).
[11] *Metal Reference Book*, 5th ed., edited by C. J. Smith (Butterworths, London, 1976).
[12] J. Garcia-Rodeja, C. Rey, and J. A. Alonso, Phys. Rev. B **49**, 8495 (1994).
[13] K. E. Schriver, J. L. Persson, E. C. Honea, and R. L. Whetten, Phys. Rev. Lett. **64**, 2539 (1990).
[14] Horngming Hsieh, R. S. Averback, Harrell Sellers, and C. P. Flynn, Phys. Rev. B **45**, 4417 (1992).
[15] Z. Pan and M. Hou, Nucl. Instrum. Methods Phys. Res. Sect. B (to be published).
[16] P. A. Montano, G. K. Shenoy, and E. E. Alp, Phys. Rev. Lett. **56**, 2076 (1986).